Geophys. J. Int. (2003) **154,** 947–956

A 3-D finite-element algorithm for DC resistivity modelling using the shifted incomplete Cholesky conjugate gradient method

Xiaoping Wu*

Department of Earth and Space Sciences, University of Science and Technology of China, Hefei 230026, *PRC. E-mail: wxp@ustc.edu.cn*

Accepted 2003 April 23. Received 2003 April 23; in original form 2002 February 25

SUMMARY

An accurate and efficient 3-D finite-element (FE) forward algorithm for DC resistivity modelling is developed. First, the total potential is decomposed into the primary potential caused by the source current and the secondary potential caused by changes in the electrical conductivity. Then, the boundary value problem for the secondary field and its equivalent variational problem are presented, where the finite-element method is used. This removes the singularity caused by the primary potential, resulting in an accurate 3-D resistivity model. Secondly, I introduce the row-indexed sparse storage mode to store the coefficient matrix and the shifted incomplete Cholesky conjugate gradient (SICCG) iterative method to solve the large linear system derived from the 3-D FE calculation. The SICCG method converges very quickly and requires much less computer storage, while the traditional ICCG or modified ICCG (MICCG) method usually fails for an irregular grid. The SICCG method is more efficient than the direct method, i.e. the elimination solver with the banded Cholesky factorization. Also, it has an advantage over the symmetric successive overrelaxation preconditioning conjugate gradient method. Numerical examples of a three-layered model with high conductivity contrast and a vertical contact show that the results from the secondary potential FE method agree well with analytic solutions. With the same grid nodes, much higher accuracy from the solution of the secondary potential than those solving the total potential can be achieved. Also a 3-D cubic body is simulated, and the dipole–dipole apparent resistivities agree well with the results from other methods.

By defining the analytical solution of a vertical contact as the primary potential, a more complicated model with several 3-D inhomogeneities near the vertical contact is simulated. The presented method also obtains good results for this model.

Key words: 3-D DC resistivity modelling, conjugate gradient method, finite element.

1 INTRODUCTION

Three principal numerical methods, namely the integral equation method (Dieter *et al.* 1969; Pratt 1972; Hohmann 1975; Lee 1975; Daniels 1977; Okabe 1981; Oppliger 1984; Xu *et al.* 1988), finite-element method (Coggon 1971; Fox *et al.* 1980; Pridmore *et al.* 1981; Holcomble & Jiracek 1984), finite-difference method (Dey & Morrison 1979; Scribe 1981; Spitzer 1995; Zhao & Yedlin 1996) are available for DC 3-D resistivity modelling. The integral equation method only considers the charge at the interface of different conductivities, so that the 3-D forward calculation requires less computer memory and is very fast. However, this method is restricted to certain model geometries and is cost effective only for small inhomogeneities. The finite-difference (FD) and finite-element (FE) methods are suitable for arbitrary 3-D structures, but an excessive storage capability and large amounts of numerical work are required for the direct method to solve the derived linear equations. The most efficient equation solver is a preconditioned conjugate gradient method combined with compact storage of the coefficient matrix. The 3-D forward problems using the FD method have been well studied by introducing, for example, the symmetric successive overrelaxation (SSOR) preconditioned conjugate gradient method (Spitzer 1995) and the incomplete Cholesky conjugate gradient (ICCG) method (Zhang *et al.* 1995; Smith 1996; Wu *et al.* 2003) as equation solvers. The amount of numerical work required in the 3-D FE resistivity modelling is larger because, the coefficient matrices are not as sparse as those from the FD method. Moreover, the finite-element matrix does not possess the property of the M-matrix (Meijerink & Van Der Vorst 1977), nor is it diagonally dominant, so that its incomplete Cholesky splitting is unstable. Thus the ICCG method used in 3-D FD modelling is not suitable for 3-D FE calculations. On the other hand, the FE method is more flexible than the FD method for

*Presently at: Institute of Geophysics, Freiberg University of Mining and Technology, Freiberg 09596, Germany. E-mail: wxp@geophysik.tu-freiberg.de

complicated geometries of electrical inhomogeneities, therefore it is necessary to develop an efficient algorithm for 3-D FE resistivity modelling.

The total potential is singular at the source point, resulting in a large error. Solving the secondary potential is an effective approach to removing the singularity effect (Xu 1994; Zhao & Yedlin 1996), the shifted incomplete Cholesky conjugate gradient (SICCG) iterative method (Manteuffel 1980) and the row-indexed sparse storage mode (Bentley 1986) are introduced to solve the large sparse linear system of equations derived from the 3-D FE computation. This greatly accelerates the convergence and reduces the storage requirements. Numerical examples show that the SICCG method is very efficient. For example, for a 2-D vertical contact model, it takes 227 iterations or about 22 s running time on a 1000 MHz Pentium computer with $39 \times 39 \times 20 = 30\,420$ nodes, while the direct method requires about 530 s. In addition, the method can also achieve much higher accuracy than solving the total potential with the same grid. For a three-layered model with a high resistivity contrast value of 1000, the average percentage error using this method is 0.28 per cent, while the average percentage error is 4.84 per cent when the total potential is solved. For a 3-D model, the dipole–dipole apparent resistivities calculated with the 3-D FE method of this paper agree well with the results presented by Pridmore *et al.* (1981).

A more complicated model with several 3-D inhomogeneities near a vertical contact is presented. Good results are obtained when the analytical solution of the vertical contact is defined as the primary potential. Comparison with the SSOR preconditioning conjugate gradient (SSORCG) method shows that SICCG is more efficient than the SSORCG method.

2 BOUNDARY VALUE PROBLEM AND EQUIVALENT VARIATIONAL PROBLEM

The fundamental differential equation of the electrical potential for the 3-D resistivity forward problem is

$$\nabla \cdot (\sigma \nabla v) = -I\delta(x, y, z), \quad \in \Omega, \tag{1}$$

where σ is the 3-D conductivity distribution, I is the current source, (x, y, z) is the Cartesian coordinate of a point in the computational domain Ω and δ is the Dirac delta function. v is the electrical potential subject to the following boundary conditions (Dey & Morrison 1979):

$$\begin{aligned} &\partial v/\partial n = 0, \quad \in \Gamma_s; \\ &\frac{\partial v}{\partial n} + \frac{\cos\theta}{r} v = 0, \quad \in \Gamma_\infty, \end{aligned} \tag{2}$$

where Γ_s is the air–earth interface, Γ_∞ is the external surface of model boundaries, θ is the angle spanned by the radial vector $\mathbf{r}$ from the source point and the outward normal direction $\mathbf{n}$ on the boundary.

However, the total potential v is singular at the source point. If v is solved for 3-D resistivity modelling, the singularity will result in a large error, especially in the neighbourhood of the source point where the singularity effects are the greatest. Xu (1994) and Zhao & Yedlin (1996) split the total potential v into the primary potential u_0 resulting from the source current in a uniform half-space of the conductive σ_0 and the secondary potential u resulting from the conductive inhomogeneities, i.e.

$$v = u_0 + u. \tag{3}$$

The primary potential u_0 satisfies

$$\nabla \cdot (\sigma_0 \nabla u_0) = -I\delta(x, y, z), \quad \in \Omega, \tag{4}$$

and its solution is

$$u_0 = \frac{I}{2\pi\sigma_0\sqrt{x^2 + y^2 + z^2}}. \tag{5}$$

From eqs (1)–(4), Xu (1994) obtained the boundary value problem for u:

$$\begin{aligned} &\nabla \cdot (\sigma \nabla u) = -\nabla \cdot (\Delta\sigma \nabla u_0), \quad \in \Omega, \\ &\partial u/\partial n = 0, \quad \in \Gamma_s, \\ &\frac{\partial u}{\partial n} + \frac{\cos\theta}{r} u = 0, \quad \in \Gamma_\infty, \end{aligned} \tag{6}$$

where $\Delta\sigma = \sigma - \sigma_0$ is the variation in the conductivity. The equivalent variational problem is given as (Xu 1994)

$$\begin{aligned} F(u) \;=\; &\int_\Omega \left[\frac{1}{2}\sigma(\nabla u)^2 + \Delta\sigma \nabla u_0 \cdot \nabla u\right] d\Omega \\ &+ \int_{\Gamma_\infty} \left[\frac{1}{2}\frac{\sigma \cos(\mathbf{r}, \mathbf{n})}{r} u^2 + \frac{\Delta\sigma \cos(\mathbf{r}, \mathbf{n})}{r} u_0 u\right] d\Gamma, \\ \delta F(u) = 0. \end{aligned} \tag{7}$$

No source term exists in eq. (7), so that the singularity has been removed by solving the secondary potential u using the finite-element method.

In fact, the primary potential u_0 in eq. (3) can be defined as the potential of any models with an analytical solution, such as a layered earth or a vertical contact. It can be easily proved from Xu (1994) that the boundary value problem for the secondary potential remains the same as eq. (6) in this situation. By defining the analytical solution of a vertical contact as the primary potential, numerical results of a complicated model with several 3-D inhomogeneities near the vertical contact will be presented to test the algorithm.

3 FINITE-ELEMENT METHOD

We only present the main steps of the 3-D resistivity finite-element method; details are reported by Pridmore *et al.* (1981), Xu (1994) and Ruan *et al.* (2001). The computational domain Ω is divided into a series of the hexahedral elements, Fig. 1 shows an arbitrary hexahedral element e. The secondary potential u within each element is interpolated by a trilinear function of the form

$$u = \sum_{i=1}^{8} N_i u_i, \tag{8}$$

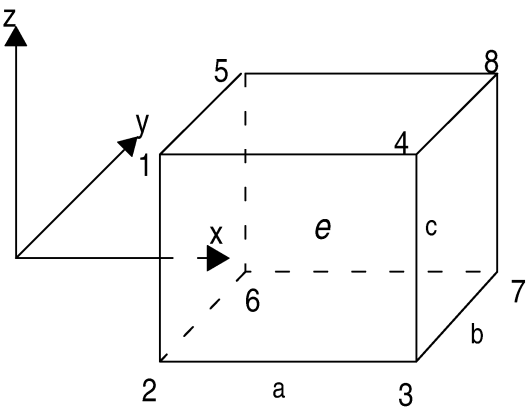

Figure 1. Illustration of the hexahedral element e for 3-D grids.

where u_i ($i = 1, 2, \ldots, 8$) are unknown nodal values of the electrical potential u and N_i ($i = 1, 2, \ldots, 8$) are shape functions defined as

$$N_i = \frac{1}{8}(1 + \xi_i\xi)(1 + \eta_i\eta)(1 + \zeta_i\zeta). \tag{9}$$

In eq. (9), ξ_i, η_i, ζ_i ($i = 1, \ldots, 8$) are the nodal values of ξ, η and ζ. The relation between ξ, η, ζ and x, y, z is

$$x = x_0 + (a/2)\xi, \quad y = y_0 + (b/2)\eta, \quad z = z_0 + (c/2)\zeta, \tag{10}$$

where (x_0, y_0, z_0) is the centre of the element and a, b, c are the length of three sides of the element e.

The integral in eq. (7) can be calculated in each element e and the boundary Γ_e. By substituting eqs (8)–(10) into eq. (7), the evaluation of each integral in eq. (7) is written as

$$\int_e \frac{1}{2}\sigma(\nabla u)^2\, d\Omega = \int_e \frac{1}{2}\sigma\left[\left(\frac{\partial u}{\partial x}\right)^2 + \left(\frac{\partial u}{\partial y}\right)^2 + \left(\frac{\partial u}{\partial z}\right)^2\right] dx\, dy\, dz = \frac{1}{2}\sigma \mathbf{u}_e^{\mathrm{T}}\mathbf{K}_{1e}\mathbf{u}_e, \tag{11}$$

$$\int_e \Delta\sigma \nabla u_0 \cdot \nabla u\, d\Omega = \int_e \Delta\sigma\left(\frac{\partial u}{\partial x}\frac{\partial u_0}{\partial x} + \frac{\partial u}{\partial y}\frac{\partial u_0}{\partial y} + \frac{\partial u}{\partial z}\frac{\partial u_0}{\partial z}\right) dx\, dy\, dz = \Delta\sigma \mathbf{u}_e^{\mathrm{T}}\mathbf{K}_{1e}\mathbf{u}_{0e}. \tag{12}$$

If one side $\overline{1234}$ of element e coincides with the external surface of boundaries Γ_∞, then

$$\frac{1}{2}\int_{\overline{1234}} \frac{\sigma \cos(\mathbf{r}, \mathbf{n})}{r} u^2\, d\Gamma = \frac{1}{2}\sigma \mathbf{u}_e^{\mathrm{T}}\mathbf{K}_{2e}\mathbf{u}_e, \tag{13}$$

$$\int_{\overline{1234}} \frac{\Delta\sigma \cos(\mathbf{r}, \mathbf{n})}{r} u_0 u\, d\Gamma = \Delta\sigma \mathbf{u}_e^{\mathrm{T}}\mathbf{K}_{2e}\mathbf{u}_{0e}, \tag{14}$$

where $\mathbf{u}_e^{\mathrm{T}} = (u_1, u_2, \ldots, u_8)$. $\mathbf{u}_{oe}^{\mathrm{T}} = (u_{01}, u_{02}, \ldots, u_{08})$. $\mathbf{K}_{1e}$ and $\mathbf{K}_{2e}$ are symmetric matrices given by (Xu 1994; Ruan *et al.* 2001)

$$\begin{bmatrix} k_{11} \\ k_{21} \\ k_{31} \\ k_{41} \\ k_{51} \\ k_{61} \\ k_{71} \\ k_{81} \\ k_{22} \end{bmatrix} = \begin{bmatrix} 4 & 4 & 4 \\ 2 & 2 & -4 \\ -2 & 1 & -2 \\ -4 & 2 & 2 \\ 2 & -4 & 2 \\ 1 & -2 & -2 \\ -1 & -1 & -1 \\ -2 & -2 & 1 \\ 4 & 4 & 4 \end{bmatrix} \begin{bmatrix} \alpha \\ \beta \\ \gamma \end{bmatrix} \quad \begin{bmatrix} k_{32} \\ k_{42} \\ k_{52} \\ k_{62} \\ k_{72} \\ k_{82} \\ k_{33} \\ k_{43} \\ k_{53} \end{bmatrix} = \begin{bmatrix} -4 & 2 & 2 \\ -2 & 1 & -2 \\ 1 & -2 & -2 \\ 2 & -4 & 2 \\ -2 & -2 & 1 \\ -1 & -1 & -1 \\ 4 & 4 & 4 \\ 2 & 2 & -4 \\ -1 & -1 & -1 \end{bmatrix} \begin{bmatrix} \alpha \\ \beta \\ \gamma \end{bmatrix}$$

$$\begin{bmatrix} k_{63} \\ k_{73} \\ k_{83} \\ k_{44} \\ k_{54} \\ k_{64} \\ k_{74} \\ k_{84} \\ k_{55} \end{bmatrix} = \begin{bmatrix} -2 & -2 & 1 \\ 2 & -4 & 2 \\ 1 & -2 & -2 \\ 4 & 4 & 4 \\ -2 & -2 & 1 \\ -1 & -1 & -1 \\ 1 & -2 & -2 \\ 2 & -4 & 2 \\ 4 & 4 & 4 \end{bmatrix} \begin{bmatrix} \alpha \\ \beta \\ \gamma \end{bmatrix} \quad \begin{bmatrix} k_{65} \\ k_{75} \\ k_{85} \\ k_{66} \\ k_{76} \\ k_{86} \\ k_{77} \\ k_{87} \\ k_{88} \end{bmatrix} = \begin{bmatrix} 2 & 2 & -4 \\ -2 & 1 & -2 \\ -4 & 2 & 2 \\ 4 & 4 & 4 \\ -4 & 2 & 2 \\ -2 & 1 & -2 \\ 4 & 4 & 4 \\ 2 & 2 & -4 \\ 4 & 4 & 4 \end{bmatrix} \begin{bmatrix} \alpha \\ \beta \\ \gamma \end{bmatrix},$$

where k_{ij} represents the entry of the matrix $\mathbf{K}_{1e}$, $\alpha = \frac{\sigma}{36}\frac{bc}{a}$, $\beta = \frac{\sigma}{36}\frac{ca}{b}$, $\gamma = \frac{\sigma}{36}\frac{ab}{c}$.

$$\mathbf{K}_{2e} = \frac{ca}{36} \cdot D \cdot \begin{bmatrix} 4 & & & & & & & \\ 2 & 4 & & & & & & \\ 1 & 2 & 4 & & & & & \\ 2 & 1 & 2 & 4 & & & & \\ 0 & 0 & 0 & 0 & 0 & & & \\ 0 & 0 & 0 & 0 & 0 & 0 & & \\ 0 & 0 & 0 & 0 & 0 & 0 & 0 & \\ 0 & 0 & 0 & 0 & 0 & 0 & 0 & 0 \end{bmatrix},$$

where $D = \cos(\mathbf{r}, \mathbf{n})/r$.

Summing up the integrals from eqs (11) to(14) within element e yields

$$F_e(u) = \frac{1}{2}\sigma \mathbf{u}_e^{\mathrm{T}}(\mathbf{K}_{1e} + \mathbf{K}_{2e})\mathbf{u}_e + \Delta\sigma \mathbf{u}_e^{\mathrm{T}}(\mathbf{K}_{1e} + \mathbf{K}_{2e})\mathbf{u}_{0e} = \frac{1}{2}\mathbf{u}_e^{\mathrm{T}}\mathbf{K}_e\mathbf{u}_e + \mathbf{u}_e^{\mathrm{T}}\mathbf{K}'_e\mathbf{u}_{0e}, \tag{15}$$

where the element matrix $\mathbf{K}_e = \sigma(\mathbf{K}_{1e} + \mathbf{K}_{2e})$, while $\mathbf{K}'_e = \Delta\sigma(\mathbf{K}_{1e} + \mathbf{K}_{2e})$. Furthermore, $\mathbf{K}_e$, $\mathbf{K}'_e$, $\mathbf{u}_e$ and $\mathbf{u}_{0e}$ are expanded to include all nodal points, and eq. (15) is written as

$$F_e(u) = \frac{1}{2}\mathbf{u}^{\mathrm{T}}\overline{\mathbf{K}_e}\mathbf{u} + \mathbf{u}^{\mathrm{T}}\overline{\mathbf{K}'_e}\mathbf{u}_0, \tag{16}$$

where $\overline{\mathbf{K}_e}$, $\overline{\mathbf{K}'_e}$, $\mathbf{u}$ and $\mathbf{u}_0$ are expanding matrices and potential vectors.

The total integral can be obtained by summing up the integrals in all elements, i.e.

$$F(u) = \sum_e F_e(u) = \frac{1}{2}\mathbf{u}^{\mathrm{T}}\sum \overline{\mathbf{K}_e}\mathbf{u} + u^{\mathrm{T}}\sum \overline{\mathbf{K}'_e}\mathbf{u}_0 = \frac{1}{2}\mathbf{u}^{\mathrm{T}}\mathbf{K}u + \mathbf{u}^{\mathrm{T}}\mathbf{K}'\mathbf{u}_0, \tag{17}$$

where $\mathbf{K} = \sum \overline{\mathbf{K}_e}$ and $\mathbf{K}' = \sum \overline{\mathbf{K}'_e}$ are global matrices of the finite element.

The functional is minimized by setting the derivative of $F(u)$ with respect to each element of $\mathbf{u}^{\mathrm{T}}$ to zero, yielding a linear system of finite-element equations

$$\mathbf{K}\mathbf{u} = -\mathbf{K}'\mathbf{u}_0, \tag{18}$$

where $\mathbf{K}$ is a sparse positive-definite and symmetric matrix (Pridmore *et al.* 1981; Xu 1994). After solving eq. (18) for the secondary potential u, the total potential v is obtained from eq. (3).

4 THE PRECONDITIONED CONJUGATE GRADIENT METHODS

4.1 Incomplete Cholesky conjugate gradient method

Let $-\mathbf{K}'\mathbf{u}_0 = \mathbf{b}$, the linear system (18) is simplified as

$$\mathbf{K}\mathbf{x} = \mathbf{b}. \tag{19}$$

The conjugate gradient (CG) procedure for solving eq. (19) is summarized as follows (Hestense & Stiefel 1952). Let $\mathbf{r}_0 = \mathbf{b} - \mathbf{K}\mathbf{x}_0$, $\mathbf{p}_0 = \mathbf{r}_0$, then

$$\alpha_i = (\mathbf{r}_i, \mathbf{r}_i)/(\mathbf{p}_i, \mathbf{K}\mathbf{p}_i),$$
$$\mathbf{x}_{i+1} = \mathbf{x}_i + \alpha_i\mathbf{p}_i,$$
$$\mathbf{r}_{i+1} = \mathbf{r}_i - \alpha_i\mathbf{K}\mathbf{p}_i, \qquad i = 0, 1, 2, \ldots,$$
$$\beta_i = (\mathbf{r}_{i+1}, \mathbf{r}_{i+1})/(\mathbf{r}_i, \mathbf{r}_i),$$
$$\mathbf{p}_{i+1} = \mathbf{r}_{i+1} + \beta_i\mathbf{p}_i \tag{20}$$

where α and β are constants, $(\mathbf{r}_i, \mathbf{r}_i)$ denotes a dot product. Eq. (20) shows that the procedure requires only the products of the matrix $\mathbf{K}$ and a vector, where the zero elements in the matrix $\mathbf{K}$ have no contribution. The row-indexed sparse storage mode is used to store non-zero elements in the lower triangular part of $\mathbf{K}$. This requires, for example, about 400 000 real storing elements for a grid of $39 \times 39 \times 20$ nodes. In contrast, the 2-D banded compact storage for the direct solution requires at least 24 000 000 real storing elements. Thus, the mathematical operations, performed only on non-zero elements for the product of $\mathbf{K}$ and a vector, reduce the time and memory requirements considerably.

However, the coefficient matrix $\mathbf{K}$ in 3-D FE resistivity modelling usually has a very large range of eigenvalues because of the irregularity of grid and the complexity of the domain of model. This means that $\mathbf{K}$ is usually very poorly conditioned. For these ill-conditioned problems, the CG algorithm converges very slowly. The efficient solver is a preconditioned conjugate gradient (PCG) method. For this purpose, the matrix $\mathbf{K}$ is split into

$$\mathbf{K} = \mathbf{M} - \mathbf{R}, \tag{21}$$

where the preconditioning matrix $\mathbf{M}$ is easily invertible and the behaviour of $\mathbf{M}$ in some sense approximates the behaviour of $\mathbf{K}$, $\mathbf{R}$ is called the error matrix and is the matrix elements omitted from the preconditioning matrix. Incomplete Cholesky decomposition is given by Varga (1960), Meijerink & Van Der Vorst (1977) and Kershaw (1978) as

$$\mathbf{M} = \mathbf{C}\mathbf{C}^{\mathrm{T}}, \tag{22}$$

where $\mathbf{C}$ is a lower triangular matrix, which can be obtained from a diagonal matrix $\mathbf{D}$ defined by

$$d_{jj} = k_{jj} - \sum_{l<j} k_{jl}^2/d_{ll}, \tag{23}$$

where k_{jl} is the elements of matrix $\mathbf{K}$. Obviously, the terms with $k_{jl} = 0$ are not included in the sum.

Then, the matrix $\mathbf{C}$ is given by

$$\mathbf{C} = \mathbf{U}\mathbf{D}^{-1/2}, \tag{24}$$

where $\mathbf{U}$ is a lower triangular matrix with $u_{jj} = d_{jj}$ for all j, $u_{jl} = k_{jl}$ for $l < j$.

The incomplete Cholesky factorization $\mathbf{C}$ is as sparse as the lower triangular of $\mathbf{K}$. It can be computed rapidly without any additional storage requirement because, non-diagonal elements of the matrix $\mathbf{U}$ are the same as those of $\mathbf{K}$.

The incomplete Cholesky factorization was first presented by Varga (1960) as a method of constructing a regular splitting of certain finite-difference operators. A quick calculation shows that $\mathbf{M}$ and $\mathbf{K}$ match each other at each non-zero element of $\mathbf{K}$. The pattern of $\mathbf{M}$ looks like that of $\mathbf{K}$ but with a few more edges, i.e. non-zero elements. The magnitude and the location of these edges determine how $\mathbf{M}$ can be taken as the approximation of $\mathbf{K}$.

If $\mathbf{C}\mathbf{C}^{\mathrm{T}}$ is an approximation for $\mathbf{K}$, eq. (19) can be rewritten as the preconditioned system

$$[\mathbf{C}^{-1}\mathbf{K}(\mathbf{C}^{\mathrm{T}})^{-1}](\mathbf{C}^{\mathrm{T}}\mathbf{x}) = \mathbf{C}^{-1}\mathbf{b}, \tag{25}$$

and the coefficient matrix $\mathbf{C}^{-1}\mathbf{K}(\mathbf{C}^{\mathrm{T}})^{-1}$ will be an approximate identity matrix, which has better condition than the original system, eq. (19). Therefore, the conjugate gradient method should converge very rapidly when applied to the matrix $\mathbf{C}^{-1}\mathbf{K}(\mathbf{C}^{\mathrm{T}})^{-1}$. Substituting the coefficient matrix $\mathbf{C}^{-1}\mathbf{K}(\mathbf{C}^{\mathrm{T}})^{-1}$ of the preconditioned system (25) into eqs (20), after a little rearrangement, the incomplete Cholesky conjugate gradient algorithm is given below:

$$\begin{aligned}
&\text{let } \mathbf{r}_0 = \mathbf{b} - \mathbf{K}\mathbf{x}_0,\ \mathbf{p}_0 = (\mathbf{C}\mathbf{C}^{\mathrm{T}})^{-1}\mathbf{r}_0, \text{ then}\\
&\alpha_i = (\mathbf{r}_i, (\mathbf{C}\mathbf{C}^{\mathrm{T}})^{-1}\mathbf{r}_i)/(\mathbf{p}_i, \mathbf{K}\mathbf{p}_i),\\
&\mathbf{x}_{i+1} = \mathbf{x}_i + \alpha_i\mathbf{p}_i,\\
&\mathbf{r}_{i+1} = \mathbf{r}_i - \alpha_i\mathbf{K}\mathbf{p}_i, \qquad i = 0, 1, 2, \ldots\\
&\beta_i = (\mathbf{r}_{i+1}, (\mathbf{C}\mathbf{C}^{\mathrm{T}})^{-1}\mathbf{r}_{i+1})/(\mathbf{r}_i, (\mathbf{C}\mathbf{C}^{\mathrm{T}})^{-1}\mathbf{r}_i),\\
&\mathbf{p}_{i+1} = (\mathbf{C}\mathbf{C}^{\mathrm{T}})^{-1}\mathbf{r}_{i+1} + \beta_i\mathbf{p}_i.
\end{aligned} \tag{26}$$

In the practical numerical procedure, the ICCG recurs until convergence criterion $|\mathbf{b} - \mathbf{K}\mathbf{x}_k|/|\mathbf{r}_0| < \varepsilon$ is satisfied, where $|\mathbf{r}_0|$ is the L2-norm of the residual in the first iteration. ε is a prespecified tolerance, which is chosen to be 10^{-8} for calculations in this paper. The success of the method depends on how well $\mathbf{C}\mathbf{C}^{\mathrm{T}}$ approximates $\mathbf{K}$. Kershaw (1978) showed that $\mathbf{M}$ is very close to $\mathbf{K}$ in the practical case of finite-difference calculations in laser fusion problems, because the eigenvalues of the matrix $\mathbf{C}^{-1}\mathbf{K}(\mathbf{C}^{\mathrm{T}})^{-1}$ are all close to 1, approximating the eigenvalues of the identity matrix. Thus, combined with the sparse storage mode of the coefficient matrix, the ICCG method has a noticeable advantage in terms of storage and time requirements over the direct solution method in solving the 3-D FD forward modelling problem (Zhang *et al.* 1995; Smith 1996; Wu *et al.* 2003).

4.2 Modified incomplete Cholesky conjugate gradient method

As ICCG proceeds through algorithms (22)–(26), it is crucial that all the d_{jj} must be larger than zero. If $d_{jj} = 0$, then the algorithm breaks off. If $d_{jj} < 0$, the algorithm may proceed, when eq. (22) is rewritten as

$$\mathbf{M} = \mathbf{U}\mathbf{D}^{-1}\mathbf{U}^{\mathrm{T}}. \tag{27}$$

However, $\mathbf{U}\mathbf{D}^{-1}\mathbf{U}^{\mathrm{T}}$ is no longer positive definite and the conjugate gradient method cannot be used to obtain the exact solution as in eqs (25) and (26) (Kershaw 1978). The ICCG for the 3-D FD resistivity modelling always gives $d_{jj} > 0$ because its coefficient matrix is positive definite, symmetric and diagonally dominant (Dey & Morrison 1979). Incomplete Cholesky decomposition of the coefficient matrix derived from 3-D FE resistivity modelling will not always give $d_{jj} > 0$ because its coefficient matrix may not be diagonally dominant. Pridmore *et al.* (1981) suggested that the diagonal dominance of an element matrix is strongly related to the degree to which the element is non-equidimensional. The more elongated an element, the smaller the degree of diagonal dominance. He also showed that the presence of a significant number of long thin elements would greatly decrease the rate of convergence of the iterative method and lead to inaccurate results. However, the presence of long thin elements is hard to avoid in 3-D resistivity modelling. If a uniform grid is employed, this means using more elements and more unknowns in the system of equations, i.e more storage and time requirements. In my experience, the ICCG iteration always breaks off while used to solve the system of 3-D FE resistivity models with an irregular grid. Therefore, the incomplete Cholesky splitting of the finite-element matrix is unstable, the ICCG method used in the 3-D FD calculation should be modified to suit the 3-D FE modelling.

Kershaw (1978) suggested a modified version of the ICCG method, that is, if $d_{jj} \le 0$ turns up, d_{jj} is simply set to some positive value as

$$d_{jj} = \sum_{l=1}^{j-1} |k_{jl}| + \sum_{l=j+1}^{m} |k_{lj}|, \tag{28}$$

and then carry on with the algorithm, eqs (22)–(26), where m is the dimension of matrix $\mathbf{K}$. He showed that if $d_{jj} \leq 0$ rarely occurs this method could work quite well for a wide variety of problems in laser fusion work. However, for the problem in 3-D resistivity FE modelling with an irregular grid, this modified ICCG iteration usually fails to achieve convergence because a large number of $d_{jj} \leq 0$ occur. The effect of the irregularity of the grid on convergence will be discussed later.

4.3 Shifted incomplete Cholesky conjugate gradient method

Manteuffel (1980) described an incomplete factorization technique for a positive-definite linear system from the implementation of the finite-element method, called the shifted incomplete Cholesky factorization. In this case, $\mathbf{K}$ is written as

$$\mathbf{K} = \mathbf{\Sigma} - \mathbf{B}, \tag{29}$$

where $\mathbf{\Sigma}$ is a diagonal matrix, composed of the diagonal elements of $\mathbf{K}$, while $\mathbf{B}$ is an off-diagonal matrix. Clearly, there is some value of μ such that the matrix $(1+\mu)\mathbf{\Sigma} - \mathbf{B}$ is diagonally dominant. Incomplete Cholesky factorization of this shifted matrix will be positive. This motivates the following splitting of $\mathbf{K}$.

Consider the matrices

$$\mathbf{K}(\mu) = \sum - \frac{1}{1+\mu}\mathbf{B}, \tag{30}$$

where $\mathbf{K}(\mu)$ represents the μ-dependent matrices and $\mathbf{K}(\mu = 0) = \mathbf{K}$. Suppose that $\mathbf{K}(\mu)$ is split into

$$\mathbf{K}(\mu) = \mathbf{M}(\mu) - \mathbf{R}(\mu), \tag{31}$$

which is similar to eq. (21). For each μ, the incomplete factorization is positive, incomplete Cholesky decomposition can be written as

$$\mathbf{M}(\mu) = \tilde{\mathbf{C}}\tilde{\mathbf{C}}^{\mathrm{T}}, \tag{32}$$

then eq. (29) is rearranged as

$$\begin{aligned}\mathbf{K} = \sum -\mathbf{B} &= \sum -\frac{1}{1+\mu}\mathbf{B} - \frac{\mu}{1+\mu}\mathbf{B} = \mathbf{K}(\mu) - \frac{\mu}{1+\mu}\mathbf{B} \\ &= \mathbf{M}(\mu) - \left[\mathbf{R}(\mu) + \frac{\mu}{1+\mu}\mathbf{B}\right] = \mathbf{M}(\mu) - \mathbf{N}(\mu),\end{aligned} \tag{33}$$

which proves to be a stable splitting of $\mathbf{K}$. The success of the splitting depends on how well $\mathbf{M}(\mu)$ approximates $\mathbf{K}$.

Let us consider the difference between $\mathbf{K}$ and $\mathbf{M}(\mu)$. For $\mu = 0$, $\mathbf{M}(\mu)$ matches $\mathbf{K}$ on the diagonal and off-diagonal non-zero of $\mathbf{K}$. In fact, it is incomplete Cholesky decomposition $\mathbf{M}$. For $\mu > 0$, $\mathbf{M}(\mu)$ also matches $\mathbf{K}$ on the diagonal, because $\mathbf{K}$ and $\mathbf{K}(\mu)$ have the same diagonal elements, but some of the errors, which are the differences between $\mathbf{M}(\mu)$ and $\mathbf{M}$, are shifted on to the off-diagonal terms of $\mathbf{M}$. In the limit, we have

$$\lim_{\mu\to\infty} \mathbf{M}(\mu) = \sum, \ \lim_{\mu\to\infty} \mathbf{N}(\mu) = \mathbf{B}, \ \lim_{\mu\to\infty} \mathbf{R}(\mu) = 0. \tag{34}$$

Thus, $\mathbf{M}(\infty)$ is equivalent to a Jacobi splitting (Manteuffel 1980). The conjugate gradient algorithm on the Jacobi splitting is equivalent to the conjugate gradient algorithm on the diagonally scaled system (Manteuffel 1980). Therefore, the shifted incomplete Cholesky factorization is possible for any positive-definite matrix, and is at least as good as the Jacobi splitting. The splitting is used in this paper, combined with the conjugate gradient method, resulting in the shifted incomplete Cholesky conjugate gradient (SICCG) algorithm.

4.4 SSOR preconditioned conjugate gradient method

Another efficient equation solver is the SSOR preconditioned conjugate gradient method. It was successfully applied to solve the 3-D FD forward problem (Spitzer 1995), which is accomplished in the following way. The positive-definite and symmetric matrix $\mathbf{K}$ is written as

$$\mathbf{K} = \mathbf{E} + \mathbf{I} + \mathbf{E}^{\mathrm{T}}, \tag{35}$$

where $\mathbf{E}$ is a lower triangular matrix and $\mathbf{I}$ is the identity matrix. Similar to eqs (21) and (22), the preconditioning matrix $\mathbf{M}$ is defined as

$$\mathbf{M} = \bar{\mathbf{C}}\bar{\mathbf{C}}^{\mathrm{T}}, \tag{36}$$

where $\bar{\mathbf{C}} = (\mathbf{I} + \omega\mathbf{E})$ and ω is a constant that denotes a relaxation factor. Then, combined with the conjugate gradient method, the algorithm similarly processes through eqs (25) and (26), resulting in the SSOR conjugate gradient method.

5 NUMERICAL EXAMPLES AND DISCUSSIONS

The test models are a three-layered earth, a 2-D vertical contact and a 3-D buried conductive cubic body. Analytical solutions are available for the first two models (Fu 1983; O'Neill & Merrick 1984). The potential is computed using the total potential finite-element (TP-FE) method and by the secondary potential finite-element (SP-FE) method, respectively, and then compared with the analytical solution to evaluate the accuracy of the SP-FE method in this study. The third model was presented by Pridmore *et al.* (1981), I recalculate the dipole–dipole apparent resistivity pseudosection and compare my results with theirs. The comparison with FD results is also presented.

The first example is a three-layered model with sharp resistivity contrast shown in Fig. 2. The top layer has a resistivity of $\rho_1 = 1\ \Omega$ m and a thickness of $h_1 = 2$ m. The middle layer has a resistivity of $\rho_2 = 1000\ \Omega$ m and a thickness of $h_2 = 2$ m. The third layer is a uniform half-space with a resistivity of $\rho_3 = 20\ \Omega$ m. A unit point source is located at the origin of the coordinate system. The analytic solution for this model is available using a digital linear filter (O'Neill & Merrick 1984). The potential for this model is calculated using the TP-FE and SP-FE method to compare with the analytic solution. In order to examine the efficiency of the SICCG solver for the FE equation system, three grids with the same size of $39 \times 39 \times 20$ but dimensions in different ratios are used in this example. The effects of irregularity on the different versions of the ICCG algorithms are shown in Table 1. For the uniform grid with $\Delta x = \Delta y = \Delta z = 0.5$ m, the coefficient matrix seems to be diagonally dominant because all d_{jj} are greater than zero for $\mu = 0$, thus the SICCG and modified ICCG methods are equivalent to the traditional ICCG method, which achieves convergence rapidly—after 60 iterations and about 10 s time. For the uniform grid with dimensions in the ratio of 4 to 1 ($\Delta x = \Delta y = 2$ m, $\Delta z = 0.5$ m), the incomplete Cholesky factorization is not positive, the traditional ICCG method breaks off because of arithmetic overflow. The modified ICCG method is able to achieve convergence only when $d_{jj} \leq 0$ seldom occurs, otherwise it fails as the traditional ICCG does. The SICCG method shows no appreciable convergence in the first 1000 iterations even with one $d_{jj} \leq 0$, however, it converges rapidly when the shifted incomplete Cholesky factorization becomes positive for $\mu \geq 0.298$. The convergence of SICCG is fastest at $\mu = 0.4$. It only requires 113 iterations and about 14 s. Even for $\mu = 30.0$ convergence still occurs within a reasonable number of iterations. As

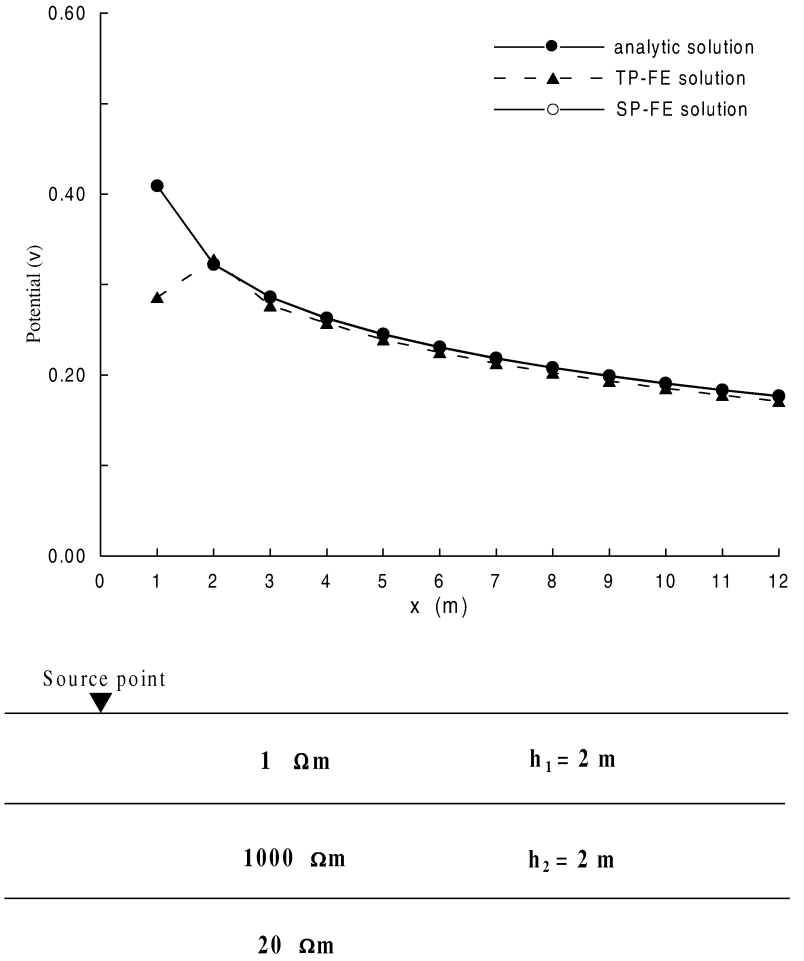

Figure 2. Comparison of the analytical and numerical solutions over a three-layered model with high resistivity contrast. The source point is located at the origin of the coordinate system.

mentioned above, it is very difficult to obtain accurate result using uniform grids for the resistivity modelling because the boundaries should be located a long distance away from the point source. Table 2 shows an irregular grid of coordinates along the x-, y- and z-axes.

Table 1. Comparison of the different versions of ICCG algorithms for grids with the same size of 39 × 39 × 20 but different dimensions.

Grids $\Delta x = \Delta y = \Delta z = 0.5$	μ	The number of $d_{ii} < 0$	ICCG iterations	MICCG iterations	SICCG iterations
	0	0	60	60	60
$\Delta x = \Delta y = 2.0$, $\Delta z = 0.5$	0	9594	Fail	Fail	Fail
	0.25	48		673	Fail
	0.27	6		409	>1000
	0.295	1		199	>1000
	0.30	0			179
	0.40	0			113
	0.80	0			135
	1.20	0			147
	2.00	0			212
	5.00	0			277
	10.00	0			302
	30.00	0			327
Irregular grid (see Table 2)	0	1306	Fail	Fail	Fail
	1.90	0			630

The SICCG method takes about 51 s to achieve convergence after 630 iterations for the irregular grid. Fig. 2 shows the comparison of analytical and numerical solutions with the 3-D FE method on this irregular grid. In spite of a high resistivity contrast value of 1000:1 in the model, the numerical results from the SP-FE method agree well with the analytic solutions. The SP-FE method is more accurate than the TP-FE method, especially in the neighbourhood of the source point where the singularity effects are the biggest. The average percentage error is 0.28 per cent for the SP-FE method and 4.84 per cent for the TP-FE method.

The second example is a 2-D vertical contact with resistivities $\rho_1 = 1\ \Omega$ m at the left-hand side and $\rho_2 = 10\ \Omega$ m at the right-hand

Table 2. Absolute coordinates along the x-, y- and z-axes of irregular grid.

Grid coordinates along x- and y-axis in metres							
−389.0	−189.0	−89.0	−39.0	−19.0	−14.0	−13.0	−12.0
−11.0	−10.0	−9.0	−8.0	−7.0	−6.0	−5.0	−4.0
−3.0	−2.0	−1.0	0.00	1.0	2.0	3.0	4.0
5.0	6.0	7.0	8.0	9.0	10.0	11.0	12.0
13.0	14.0	19.0	39.0	89.0	189.0	389.0	
Grid coordinates along z-axis in metres							
0.00	0.50	1.0	1.5	2.0	3.0	4.0	5.0
6.0	7.0	8.0	9.0	13.0	17.0	23.0	33.0
53.0	103.0	203.0	403.0				

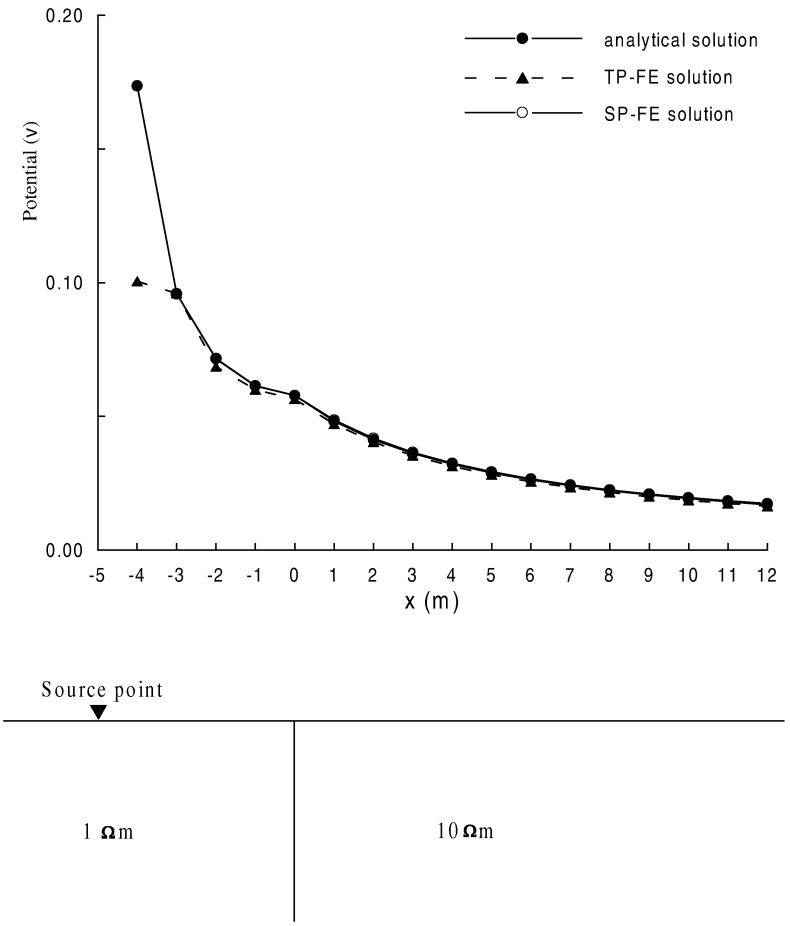

Figure 3. Comparison of the analytical and numerical solutions over a vertical contrast, the point source is located at 5 m offset from the contact plane, i.e. $x = -5$ m, $y = 0$ m and $z = 0$ m.

side. A unit point source is located 5 m left from the contact plane, i.e. $x = -5$ m, $y = 0$ m and $z = 0$ m. The grid also consists of 39 × 39 × 20 nodes and has a similar structure to that shown in Table 2. Fig. 3 shows the model and the comparison of analytical and numerical solutions with the 3-D FE method. The SP-FE method also gives more accurate results than the TP-FE method. The numerical solution by the SP-FE method has an average error of 0.54 per cent, while the average error of solutions by the TP-FE method is 6.37 per cent. Besides, the SICCG iterative method with $\mu = 1.0$ takes only about 22 s for 227 iterations, however, it requires about 530 s when the direct method is used to solve the finite-element equations. This is about 24 times faster than the direct method. Fig. 4 shows the number of iterations required to reach the convergence for various values of μ. It is found that the factorization is not positive for $\mu \leq 0.591$ and convergence is fastest in the vicinity of $\mu = 1.0$.

The third model is a buried cubic body of side 2 m, with a depth of 0.5 m below the surface of the earth. The surrounding host rock has a resistivity of 100 Ω m and the inhomogeneity has a resistivity of 20 Ω m. Pridmore *et al.* (1981) illustrated a comparison of its apparent resistivities calculated by the finite-element and integral-equation (IE) methods, the results from the two methods agree to within about 6 per cent. However, the result from the integral-equation method seems to be more accurate because the apparent resistivities calculated from the integral-equation method satisfy reciprocity well, but the results obtained from the finite-element method satisfy reciprocity to within 6 per cent. For a 3-D grid of 49 × 29 × 18 in this study, the SICCG method takes approximately 20 s for 200 iterations for each of the seven source positions with $\mu = 2.0$. The dipole–dipole apparent resistivity pseudo-sections for a profile over the centre of inhomogeneity are illustrated in Fig. 5. The above values of each line in Fig. 5 illustrate apparent resistivities calculated from the present SP-FE method, while the middle and below values illustrate the results from TP-FE and IE methods by Pridmore *et al.* (1981), respectively. The results from the SP-FE method agree well with those from the IE method, the maximum error between them

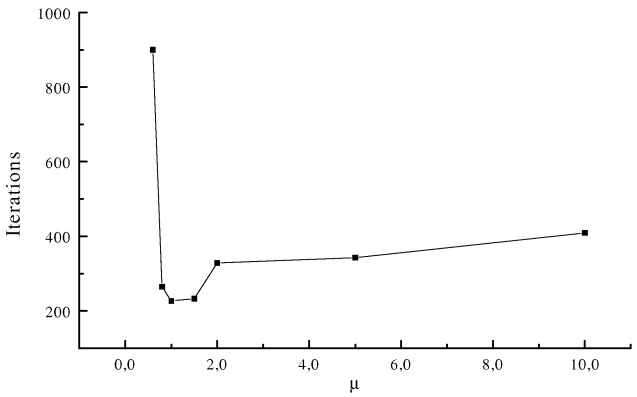

Figure 4. Iterations to convergence for various values of μ.

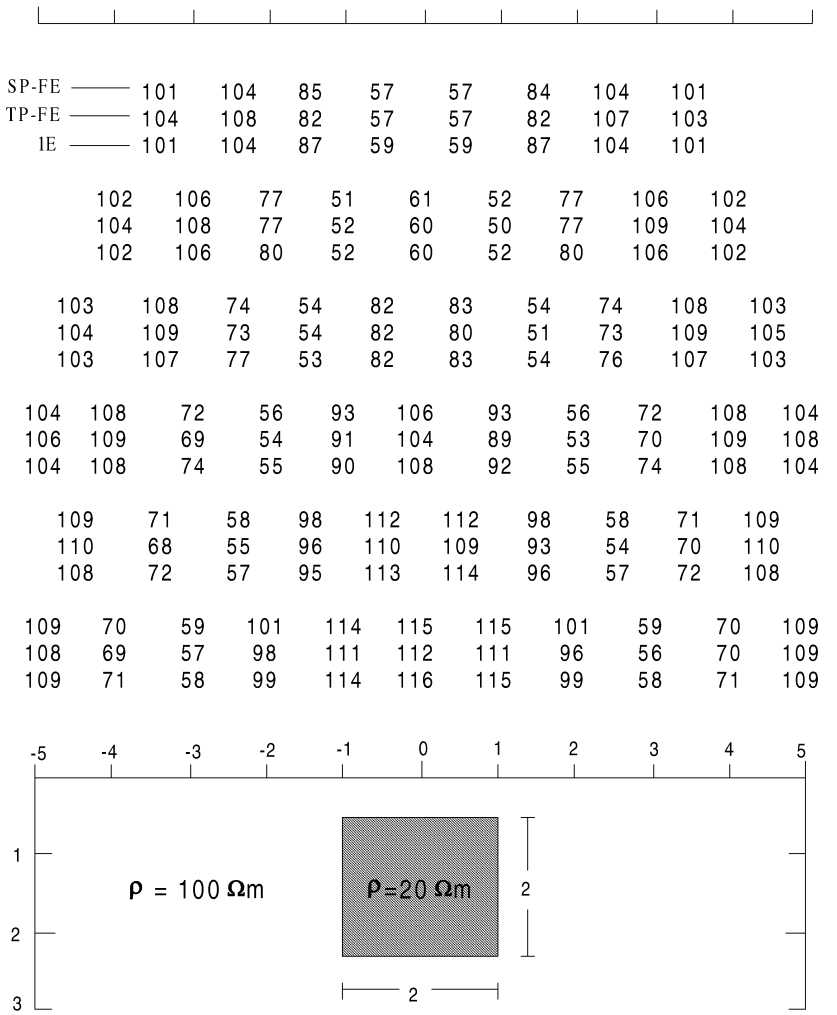

Figure 5. Comparison of dipole–dipole apparent resistivities calculated by the secondary potential finite-element, total potential finite-element and integral equation methods over a 3-D body. The values shown are apparent resistivities in Ω m. The model, as well as the results of TP-FE and IE methods, is taken from Pridmore *et al.* (1981), used with permission.

is only 3.9 per cent, while the maximum error between TP-FE and IE results is 6.8 per cent. Finally, this numerical experiment again confirms that the SP-FE method gives more accurate results than the TP-FE method.

As above, the presented method works well in terms of efficiency and accuracy. On the other hand, it can be seen that high conductivity contrast in the model has an effect on the convergence rate of SICCG iteration. In the first example with higher conductivity contrast, SICCG takes more time and iterations to achieve convergence. As we know, the pattern of the finite-element matrix depends on the irregularity of the grid and the complexity of the domain of the model which denotes the conductivity distribution as well as the conductivity contrast. The more irregular the grid and the higher the conductivity contrast, the more ill-conditioned the coefficient matrix, and the slower the iterative method converges.

Fig. 6 shows the comparison of the SP-FE method of this paper with the secondary potential finite-difference (SP-FD) method (Wu *et al.* 2003) for a model presented by Pridmore *et al.* (1981). The model is a hypothetical massive sulphide model with a resistivity of 10 Ω m, where the mineralization is adjacent to a contact between two different rock units and is covered by irregular, conductive overburden (see Fig. 6). The rock resistivities at two sides of the contact are 100 and 300 Ω m, while the strike length of the other features in the model is shown in brackets. For this model, I calculate the dipole–dipole apparent resistivities using the SP-FE and SP-FD methods by defining the analytical solution of the vertical contact as the primary potential. Fig. 6(a) illustrates the comparison between the results calculated by two methods for the fault (contact) plus the massive sulphide body, while Fig. 6(b) illustrates the comparison of the results for the model with all components. The results from both methods agree well, the average error is less than 1.0 per cent for the dipole–dipole apparent resistivity in Fig. 6(a) and less than 2 per cent for apparent resistivities in Fig. 6(b). Also the results from both SP-FE and SP-FD methods are close to those from the TP-FE method by Pridmore *et al.* (1981). It shows that the algorithm is effective while considering a more complicated model for the primary potential.

A comparison of the computing efficiency of SICCG and SSORCG algorithms is made for this model. The grid consists of $57 \times 39 \times 18 = 40\,014$ nodes. Numerical tests show that $\omega = 2.0$ is the optimal value of the relaxation parameter for the SSORCG method and $\mu = 1.4$ is the optimal value for the SICCG method. With the optimal values, the SICCG method takes an average of 20 s

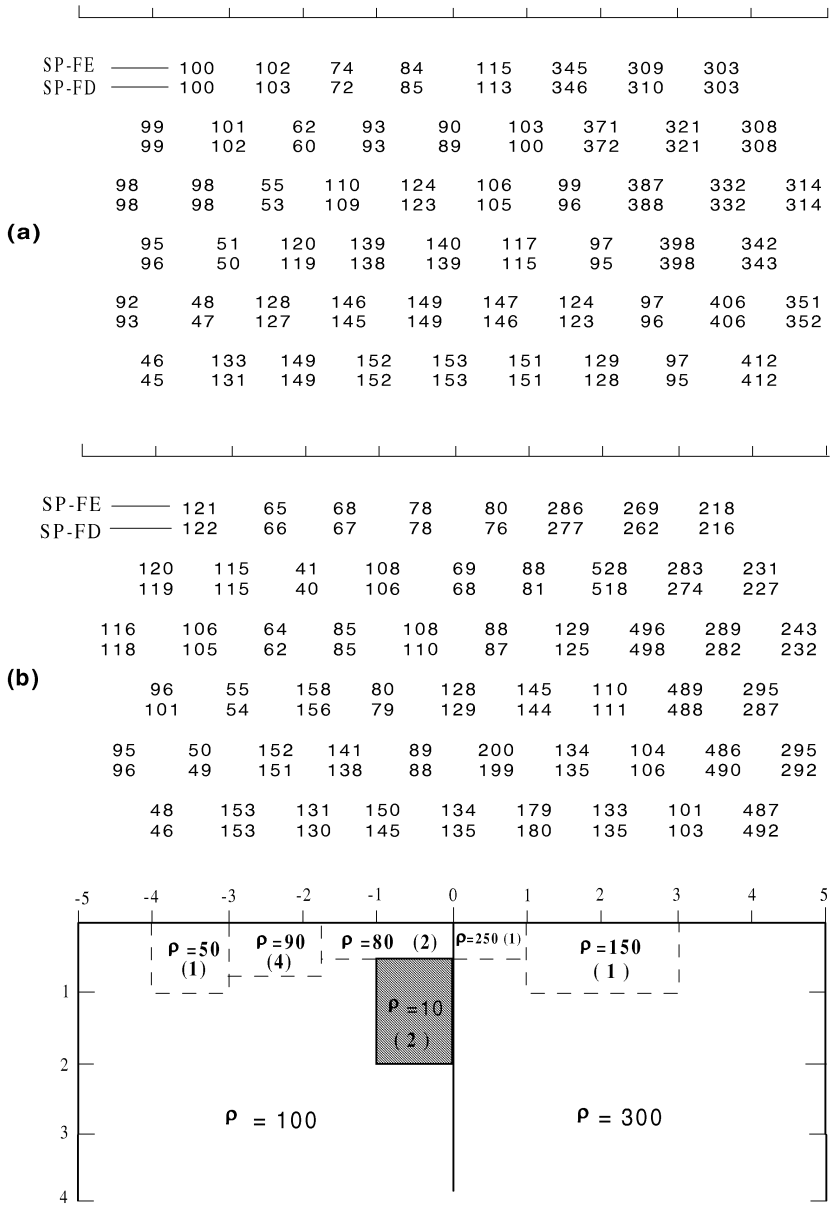

Figure 6. Comparison of dipole–dipole apparent resistivities calculated by SP-FE and SP-FD methods over a complicated model by defining the analytical solution of the vertical contact as the primary potential. (a) Vertical contact and massive sulphide, (b) all components of the model. The model is taken from Pridmore *et al.* (1981), used with permission. All values are in Ω m.

and 135 iterations for each of the seven source positions, while the SSORCG method requires an average of 30 s and 230 iterations.

6 CONCLUSION

In this paper, an accurate and efficient 3-D FE forward algorithm for DC resistivity modelling is presented. The novelty of the method lies in the application of the SICCG iterative accelerator combined with the row-indexed sparse storage mode to the solution of the secondary potential. The presented algorithm is more efficient than the direct method in terms of storage and time requirements, and also has an advantage over the SSORCG method. Numerical results show that the secondary potential finite-element method can achieve higher accuracy than the total potential finite-element method. Using a complicated model for the primary potential can further reduce the singularity of the potential and make the solution more stable.

ACKNOWLEDGMENTS

This work was carried out in China and supported by the Natural Sciences Foundation of China (no 40004005) and the Ministry of Land & Resources, PRC. I would like to thank Dr Ashok Agarwal and an anonymous reviewer for their excellent comments, and the editor, Professor Karsten Bahr for many encouragements. The author also thanks Professor K. Spitzer, Freiberg University of Mining and Technology, Germany, for his helpful suggestions.

REFERENCES

Bentley, J., 1986. *Programming Pearls,* pp. 87–98, Addision-Wesley, Reading.

Coggon, J.H., 1971. Electromagnetic and electrical modeling by the finite element method, *Geophysics,* **36,** 132–155.

Daniels, J.J., 1977. Three-dimensional resistivity and induced polarization modeling using buried electrodes, *Geophysics,* **42,** 1006–1019.

Dey, A. & Morrison, H.F., 1979. Resistivity modeling for arbitrarily shaped three-dimensional structures, *Geophysics,* **44,** 753–780.

Dieter, K., Paterson, N.R. & Grant, F.S., 1969. IP and resistivity type curves for three-dimensional bodies, *Geophysics,* **34,** 615–632.

Fox, R.C., Hohmann, G.W., Killpack, T.J. & Rijo, L., 1980. Topographic effects in resistivity and induced-polarization surveys, *Geophysics,* **45,** 75–93.

Fu, Liangkui, 1983. *Lecture of Geoelectrical Prospecting Methods,* pp. 50–56, Geology Press, Beijing.

Hestense, M. & Stiefel, E., 1952. Methods of conjugate gradients for solving linear systems, *J. Res. Nat. Bur. Standards,* **49,** 409–436.

Hohmann, G.W., 1975. Three-dimensional induced polarization and electromagnetic modeling, *Geophysics,* **40,** 309–324.

Holcomble, H.T. & Jiracek, G.R., 1984. Three-dimensional terrain correction in resistivity surveys, *Geophysics,* **49,** 33–59.

Kershaw, D.S., 1978. The incomplete Cholesky-conjugate gradient method for the iterative solution of systems of linear equations, *J. Comp. Phys,* **26,** 43–65.

Lee, T., 1975. A integral equation and its solution for some two- and three-dimensional problem in resistivity and induced polarization, *Geophys. J. R. astr. Soc.,* **42,** 81–95.

Manteuffel, T.A., 1980. An incomplete factorization technique for positive definite linear systems, *Math. Comp,* **34,** 473–497.

Meijerink, J.A. & Van Der Vorst, H.A., 1977. An iterative solution method for linear system of which the coefficient matrix is a symmetric matrix, *Math. Comp.,* **31,** 148–162.

Okabe, M., 1981. Boundary element method for arbitrary inhomogeneities problem in electrical prospecting, *Geophys. Prospect.,* **29,** 39–59.

O'Neill, D.J. & Merrick, N.P., 1984. A digital linear filter for resistivity sounding with a generalized electrode array, *Geophys. Prospect.,* **32,** 105–123.

Oppliger, G.L., 1984. Three-dimensional terrain corrections for mise-a-la-masse and magnetometric resistivity surveys, *Geophysics,* **49,** 1718–1729.

Pratt, D.A., 1972. The surface integral approach to the solution of the 3-D resistivity problem, *Bull. Austral., Soc. Expl. Geophys.,* **3,** 33–50.

Pridmore, D.F., Hohmann, G.W., Ward, S.H. & Sill, W.R., 1981. An investigation of finite element modeling for electrical and electromagnetic data in three dimensions, *Geophysics,* **46,** 1009–1024.

Ruan, B.Y., Xiong, B. & Xu, S.Z., 2001. Finite element method for modeling resistivity sounding on 3-D geoelectric section, *Earth Sci.,* **26,** 73–77 (in Chinese).

Scribe, H., 1981. Computations of the electrical potential in the three-dimensional structure, *Geophys. Prospect.,* **29,** 790–802.

Smith, J.T., 1996. Conservative modeling of 3-D electromagnetic fields, Part II: biconjugate gradient solution as an accelerator, *Geophysics,* **61,** 1319–1324.

Spitzer, K., 1995. A 3-D finite difference algorithm for DC resistivity modeling using conjugate gradient methods, *Geophys. J. Int.,* **123,** 903–914.

Varga, R.S., 1960. Factorization and normalized iterative methods, in *Boundary Problems in Differential Equations,* ed. Langer, R.E., Univ. of Wisconsin Press, Madison.

Wu, X.P., Xiao, Y.F., Qi, C. & Wang, T.T., 2003. Computations of secondary potential for 3-D dc resistivity modeling using incomplete Cholesky conjugate gradient method, *Geophys. Prospect.* accepted.

Xu, S.Z., 1994. *FEM in Geophysics,* pp. 178–193, Science Press, Beijing (in Chinese).

Xu, S.Z., Guo, Z.C. & Zhao, S.K., 1988. An integral formulation for three-dimensional terrain modeling for resistivity surveys, *Geophysics,* **53,** 546–552.

Zhang, J., Mackie, R.L. & Madden, T.R., 1995. Three-dimensional resistivity forward modeling and inversion using conjugate gradients, *Geophysics,* **60,** 1313–1325.

Zhao, S.K. & Yedlin, M.J., 1996. Some refinements on the finite-difference method for 3-D dc resistivity modeling, *Geophysics,* **61,** 1301–1307.